ORIGINAL PAPER

Sustainable thin-wall machining: holistic analysis considering the energy efficiency, productivity, and product quality

Gururaj Bolar[1] · Shrikrishna N. Joshi[2] · Sanghamitra Das[2]

Abstract

Enhanced energy efficiency, product quality, and productivity have become crucial requirements in thin-wall machining. Therefore, the work examined the impact of axial depth of cut, radial depth of cut, feed per tooth, and tool diameter on three performance measures. Full factorial was used to design experiments, and Analysis of Variance (ANOVA), a statistical method, was employed to analyze and interpret the influence of process variables on the machining performance. Additionally, Non-Dominated Sorting Genetic Algorithm-II (NSGA-II) was adopted to arrive at the Pareto-optimal solutions to evaluate the trade-off between the three performance measures. The optimized process parameters for roughing operation helped maximize the process productivity at the expense of product quality. In contrast, the Pareto solutions for finishing operation effectively improved energy efficiency and produced quality open straight and curved thin-wall parts. Improved surface finish with minimal deflection can be achieved by milling with a cutter of diameter 8 mm and maintaining the feed, axial, and radial depth at 0.02 mm/z, 8 mm, and 0.3125 mm, respectively. The proposed findings can provide effective solutions for machining open straight and curved thin-wall parts with improved productivity, product quality, and energy efficiency.

Keywords Thin-wall machining · Productivity · Product quality · Cutting power · Optimization

1 Introduction

Modern aviation manufacturers are incorporating thin monolithic structures to improve aircraft's durability and fuel efficiency. Considering the massive removal of material that accounts for 90–95% of the initial volume, enhancement in the process productivity is vital [1]. However, increasing the process productivity by incorporating sub-optimal machining conditions can result in substandard surface quality and poor dimensional accuracy. Furthermore, energy efficiency has become a key phrase and an integral part of sustainable manufacturing [2]. Therefore, the optimized machining parameters must be at disposal while machining thin-wall parts to obtain excellent product quality and enhanced productivity while reducing power consumption.

Several comprehensive studies emphasizing the optimization of the CNC milling process have been reported. Rajeswari and Amirthagadeswaran [3] analyzed the responses like tool wear, cutting force, surface roughness, and material removal rate using Response Surface Method (RSM) when machining aluminum metal matrix composite. The analysis revealed the weight% of SiC and spindle speed as significant factors influencing machinability. Conflicting performance variables were then optimized using Grey Relational Analysis (GRA). The influence of tool overhang length and surface inclination angle on cutting forces and vibration while milling hardened steel was investigated by Wojciechowski et al. [4]. The process variables had a significant impact on the forces and vibrations. Further, GRA was applied, and optimal process variables were established for minimizing the vibrations and cutting forces. Pa et al. [5] directed a study to ascertain the influential process parameters affecting the surface quality while ball end milling 2.5D components. Surface quality was affected by the axial depth of cut magnitude. Taguchi-based optimization revealed that

✉ Gururaj Bolar
gururaj.bolar@manipal.edu; gururaj.bolar@gmail.com

1   Department of Mechanical and Manufacturing Engineering, Manipal Institute of Technology, Manipal Academy of Higher Education, 576 104 Manipal, Karnataka, India

2   Department of Mechanical Engineering, Indian Institute of Technology Guwahati, 781 039 Guwahati, Assam, India

lower axial depth of cut, lower feed rate, higher spindle speed, and higher surface inclination angle were the best choice to obtain a superior surface finish. Ren et al. [6] made an attempt to determine the optimal end mill geometry for milling titanium alloy. The process variable considered was helix angle, radial rake angle, and primary radial relief angle, while the performance measures were surface roughness and residual stress. The experimental results showed radial rake angle as the critical factor affecting surface integrity. After the optimization, a significant improvement in surface integrity was reported. Tlhabadira et al. [7] evaluated the effect of feed, depth of cut, and cutting speed on the surface finish while milling AISI P20 steel. Additionally, the Taguchi method was used to optimize surface roughness while milling AISI P20 steel. Lower cutting speeds helped in maintaining a good surface finish. Sarıkaya et al. [8] deliberated on the influence of process variables on cutting force, surface roughness, and vibration signals. Additionally, the optimum values of process variables were estimated using GRA. Feed rate was identified as the most critical parameter affecting the machining performance. Jomaa et al. [9] attempted to identify the optimal process parameters using GRA to improve the surface finish characteristics of the aluminum alloy during peripheral milling. The influence of feed per tooth, radial depth of cut, cutting speed, milling mode, and cutting tool geometry on the surface roughness was investigated. All the process variables significantly affected the quality of the milled surface. An attempt was made to determine the optimal process variables.

Karabulut et al. [10] deliberated on the selection of process variables for better surface quality while milling aluminum metal matrix composite. Further, Artificial Neural Network (ANN) was adopted to develop the prediction models. The finish of the machined surface was affected by the built-up edge formation and interfacial bonding of reinforcement particles. Moreover, cutting speed and feed rate were established as essential parameters to control surface quality. Campatelli et al. [11] investigated the contribution of cutting speed, depth of cut, and feed rate on energy consumption during end milling and optimized the process considering the energy minimization criterion. The results were evaluated using Response Surface Method (RSM). The analysis demonstrated that increasing the material removal rate (MRR) lowered the environmental footprint, and the same could be accomplished by optimizing the cutting speed and feed rate. Jang et al. [12], as a part of environmentally conscious manufacturing, analyzed and optimized the specific cutting energy during milling using Particle Swarm Optimization (PSO). The model was developed by considering flow rate, feed rate, depth of cut, and cutting speed as process variables. The model could accurately predict the cutting energy with less than 1% error.

Likewise, Zhang et al. [13] investigated the impact of process parameters on carbon emissions and power consumption while milling medium carbon steel. The empirical models were developed using Principal Component Analysis (PCA), and optimized process parameters were ascertained following a multi-objective optimization approach. The results showed that a larger feed rate and larger depth of cut improved the machining performance. Ahmed and Arora [14] investigated cutting velocity, cutting depth, and feed rate effects on energy consumption and surface roughness when end-milling plain low-carbon steel. The impact of process variables was evaluated using the analysis of variance. Moreover, an ANN-based predictive model was utilized to assess energy consumption and surface roughness. Further, GA was adopted to optimize the conflicting multi-objectives. Nguyen et al. [15] analyzed the influence of tool radius, feed, depth of cut, and cutting speed on product quality and energy efficiency. All the process variables were found to influence the two performance measures. Further, an attempt was made to enhance energy efficiency and product quality while milling stainless sheet 304. Neural Network (NN) was adopted to correlate the input and output parameters, and the optimal process parameters were determined using Adaptive Simulated Annealing (ASA) algorithm. A considerable improvement in the milling responses was noted when the optimized process variables were employed. Kar et al. [16] made an attempt to study the influence of process variables on material removal rate, cutting force, and surface roughness. Desirability Function Analysis (DFA) was also utilized to optimize the process. Collected responses were converted to individual desirability, and the fuzzy inference was utilized to change individual desirability values to a multi-performance character index (MPCI). The optimal process variables were determined by maximizing the MPCI. Wang et al. [17] evaluated the energy consumption and productivity during milling by varying the process variables, including axial depth of cut, feed rate, spindle speed, and radial depth of cut. Further, Artificial Bee Colony (ABC) intelligent algorithm was applied to optimize the multi-objective problem.

The researchers have made a few endeavors to optimize the thin-wall milling process. Ghoddosian et al. [18] analyzed the influence of cutting variables like the width of cut, feed rate, and spindle speed on the surface roughness of milled aluminum thin-wall. Additionally, the process was optimized using the Genetic Algorithm (GA) and Imperialist Competitive (IC) algorithm. Songtao et al. [19] examined the cutting forces by varying the important process variables, including feed rate, cutting speed, radial and axial depth cut. Selected process variables influenced the cutting forces. It was reported that cutting forces causing the wall deformation were effectively controlled by selecting smaller

axial cuts and bigger radial cuts at high cutting speeds. Qu et al. [20] made an attempt to optimize the conflicting objectives, including surface roughness, and material removal, using a multi-objective optimization strategy. The objective functions were determined using regression analysis, and optimal machining parameters to enhance the quality and productivity were determined using NSGA-II. Ringgaard et al. [21] made an attempt to optimize the thin-wall machining process by maximizing the material removal rate. The researchers considered chatter stability and forced vibration as constraints and used the penalty cost function approach to optimize the process. An investigation was conducted by Cheng et al. [22] to determine the effect of depth of cut, feed rate, and spindle speed on surface roughness during thin-wall machining. The outcome of the study showed that feed rate and spindle speed significantly impacted the surface roughness, whereas the depth of cut influenced the wall deformation. Finally, the ABC algorithm was employed to determine the optimal process variables. The reviewed literature clarifies that optimization of the bulk milling process has always been a critical research area. Several attempts have been made to improve the various performance characteristics during the bulk milling operation. The literature also reveals a few attempts to optimize the performance of the thin-wall machining process by considering product quality and productivity. However, the analysis and optimization of energy consumption for the thin-wall machining process remain unexplored. Moreover, very limited literature is available on the integrated optimization approach of thin-wall machining process considering the surface roughness, wall deflection, material removal rate and cutting power.

Therefore, the present work investigates the influence of the process variables, namely tool diameter, axial depth, radial depth, and feed per tooth, on productivity (material removal rate), product quality (surface roughness and wall deflection), and energy efficiency (cutting power). The significance of process parameters was assessed using Analysis of Variance (ANOVA). Mathematical models to relate the process variables and performance measures were developed using regression analysis. Additionally, multi-objective-based process optimization was performed in order to optimize the thin-wall machining process by maximizing productivity and product quality while minimizing the cutting power. Considering the conflicting nature of the objectives, NSGA-II was utilized to determine the optimal levels of process parameters. The optimal parameters ascertained from the optimization process were validated using experiments. The outcomes of the present work provide a wide range of solutions for machinists and decision-makers who are involved in the machining and production of thin-wall structures. The central findings provide an effective solution
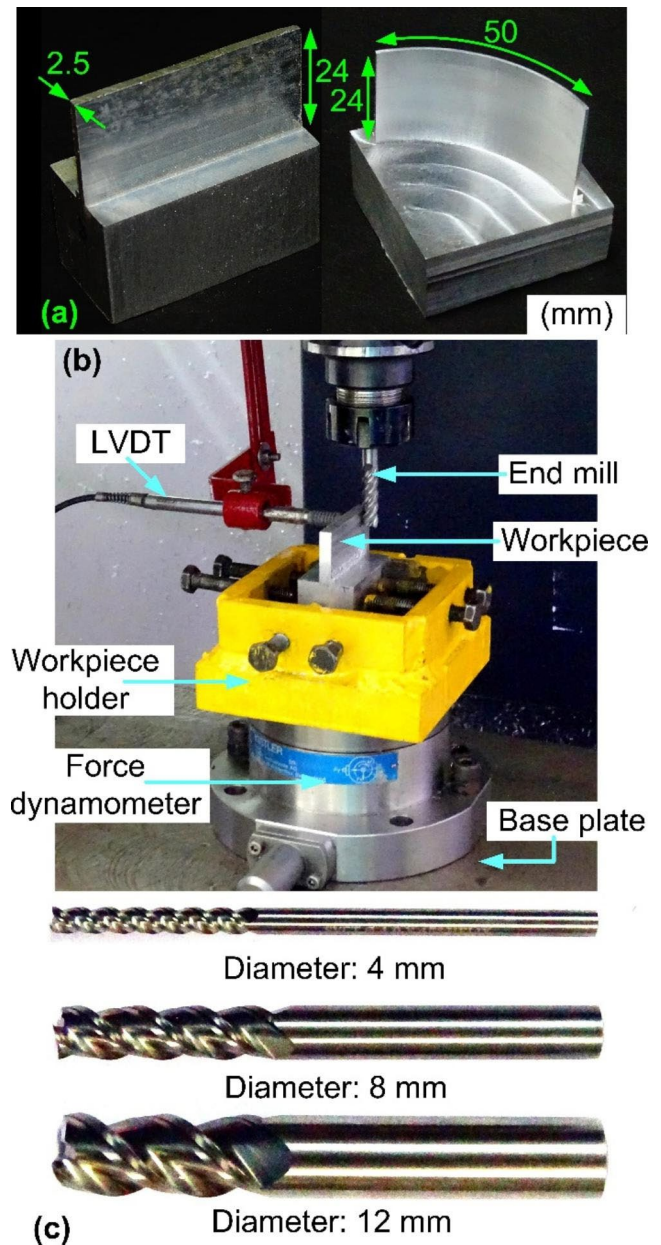

Fig. 1 (a) Thin-wall specimens, (b) Experimental set-up, (c) End milling tools

for machining open straight and curved thin-wall parts, especially when high productivity, product quality, and energy efficiency are mandated.

2 Experimental methods

The machining experiments were performed by milling aluminum alloy 2024-T351 specimens (see Fig. 1(a)) on a CNC vertical machining center (*PMK model: MC-3/400*) using the set-up shown in Fig. 1(b). The wall thickness was reduced for the evaluation from 2.5 mm to 1.25 mm. Solid

Fig. 2 **(a)** Chatter marks in the finished workpiece (BUE), **(b)** Built-up-edge formation
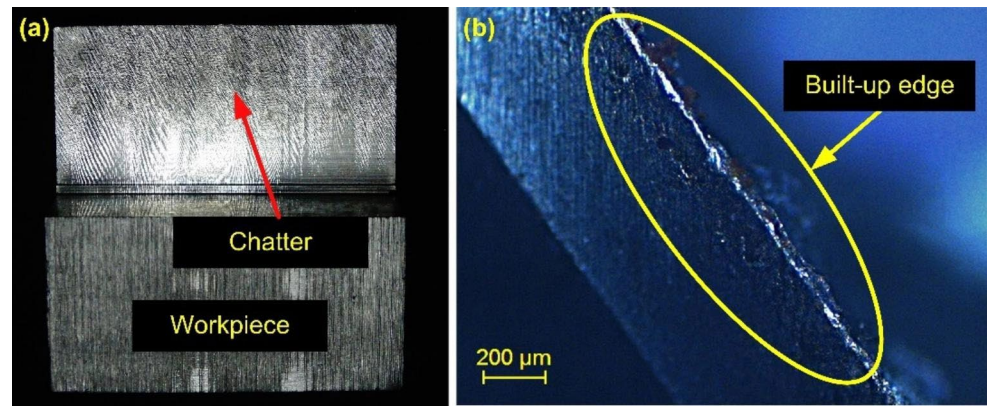
carbide flat-bottom end mills were considered for machining experiments (Fig. 1(c)). In the present work, an environment-friendly dry mode of cutting was chosen to carry out extensive investigations. The study aims to improve the thin-wall process productivity and simultaneously lower the power consumption, surface roughness, and in-process wall deflection. Usually, enhancement in productivity, i.e., an increase in material removal rate, is generally achieved by employing maximum possible levels of process parameters, viz., spindle speed, depth of cuts, and feed rate. However, machining at these high levels often produces dimensionally inaccurate thin-wall parts with poorer surface quality. Moreover, the low modulus of elasticity of the aluminum alloy can cause the thin-wall to deflect during the final stages of machining, leading to part deformation and vibration-induced chatter. Chatter can lead to a poor surface finish which again might lead to part rejection, thus lowering productivity and increasing the cost. Thus, selecting proper levels of milling parameters is crucial as they influence the dimensional accuracy, material removal rate, milling forces, and surface finish. Therefore, screening experiments were performed to decide on the levels of process variables. The process parameters for screening experiments were cutting speed, feed per tooth, axial, and radial depth of cut. For the investigation, cutting speeds of 63 m/min, 88 m/min and 113 m/min were chosen. During the investigation, chatter marks were formed at a cutting speed of 113 m/min (Fig. 2(a)). While the employment of a lower cutting speed of 63 m/min resulted in built-up-edges (BUEs) formation (see Fig. 2(b)). Moreover, the surface quality suffered due to the persistent BUE formation. Since the machining condition (88 m/min) showed stable machining, it was decided to include the cutting speed for further analysis. During the experimentation, the feed per tooth was varied from 0.06 mm/z to 0.1 mm/z. It was noted that employment of higher values (0.08 mm/z and above) showed signs of BUE formation and surface deterioration. Therefore, it was thought worth conducting further investigations to study the influence of feed on the response parameters while

maintaining the feed value below 0.06 mm/z. Regarding the axial and radial depth of cut, Sandvik-Coromant and Boeing Research and Technology group reported that selecting proper machining strategies, viz., radial depth of cut and axial depth of cut, is a key to efficient thin-wall machining. Accordingly, from the initial experiments, it was noted that the axial and radial depth of cut significantly influenced the cutting forces, surface roughness, and wall deflection. Moreover, literature reports scant research on the influence of radial depth of cut on thin-wall deflection, milling force, and surface quality. Additionally, the productivity of the thin-wall machining process is a function of axial and radial depth of cut. Therefore, it was decided to study the influence of axial and radial depth of cut on the process performance, and the levels were set considering to maximize the process productivity. In the present study, the radial depth of cut was varied considering the roughing and finish cutting conditions. Smaller width of cut was selected for finish cut, while a larger width of cut was utilized for roughing operation. The width of cut varied between 0.3125 and 1.25 mm.

A preliminary study was also performed to determine the impact of tool diameter on surface roughness and cutting forces. Tools of different diameters (8 mm, 12 mm, and 16 mm) were selected for the study. The results showed that the cutting forces and surface roughness increased drastically when an end mill 16 mm diameter was used to machine the thin-wall. Based on the outcome, 16 mm end mills were excluded from further studies. The preliminary study showed that 8 mm tools provided a significantly better result in terms of lower cutting forces and surface roughness. Because a smaller diameter tool provided better results, it was decided that a smaller diameter tool be included in the present study. As a result, a 4 mm diameter end mill was considered for further evaluation. Additional details with regard to the selection of tool diameter can be obtained in [23]. The cutting speed in the presented study varied between 44 and 132 m/min. Accordingly, the finalized process variables and the levels are listed in Table 1.

Table 1 Process parameters and their levels

Process parameters	Level 1	Level 2	Level 3
Tool diameter, d_t(mm)	4	8	12
Feed per tooth, f_z(mm/z)	0.02	0.04	0.06
Axial cut depth, a_d(mm)	8	12	24
Radial cut depth, r_d(mm)	0.3125	0.625	1.25

A non-contact profilometer (*Taylor Hobson Talysurf CCI Lite*) measured the surface roughness (R_a). The profilometer has an objective lens of 20× magnification and a focal distance of 4.7 mm. The collected profile was analyzed using *TalyMap*. The measurement was carried along the tool feed direction. The measurement was taken at seven locations, and the average was considered in the study. The measuring system and a sample 3-D profile are shown in Fig. 3(a). The in-process wall deflection (D_f) was measured in-process using Linear Variable Differential Transformer (LVDT) (*Solartron AX/5/S*). The LVDT was mounted on a holder which moved with the machine spindle. The reading was obtained using a digital display (*Solartron C55*). The deflection measurement procedure is shown in Fig. 3(b). Cutting force components were measured using a piezoelectric dynamometer (*Kistler 9272B*). The dynamometer has a measurement range of − 5 to + 5 kN. The measured data was conditioned using a charge amplifier (*Kistler make, Model: 5070 A*). The signal was further analyzed using data analysis software (*DynoWare: 2825 A*). During the measurement, the sampling rate was set at 2000 Hz/Channel, and the measurement was made for a duration of 15 s. The three cutting force components, F_x, F_y, and F_z were measured based on the dynamometer-specified reference system. The cutting force measurement system is shown in Fig. 3(c). The MRR was computed by calculating the machining time and actual volume of material removed.

Experiments were performed following a full factorial design (3^4 experiments). The experimental results and the significance of thin-wall milling variables on product quality, productivity, and cutting power were analyzed using ANOVA. The contribution of the process variables to the performance measures was evaluated by carrying out P and F values tests at a 95% confidence level. A P-value smaller than 0.05 indicates that the process variable is significant [24]. The process variables were correlated with the responses using second-order regression equations. A generalized second-order polynomial model is given as:

$$y = \delta_0 + \sum_{i=1}^{k} \delta_i x_i + \sum_{i<j} \sum \delta_{ij} x_i x_j + \sum_{i=1}^{k} \delta_{ii} x_i^2 + \varepsilon \quad (1)$$

where y is the predicted response, ε is the random deviation, δ_0 a constant, δ_i, δ_{ii} and δ_{ij} are the first and second-degree input parameters and parameter interactions, respectively [25].

While solving multi-objective optimization problems, it is impossible to consider a single solution as the best result. Optimized levels of process variables determined for one performance measure need not be suitable for achieving the targeted performance for another output. Hence, it becomes essential to decide on a wide range of solutions from which
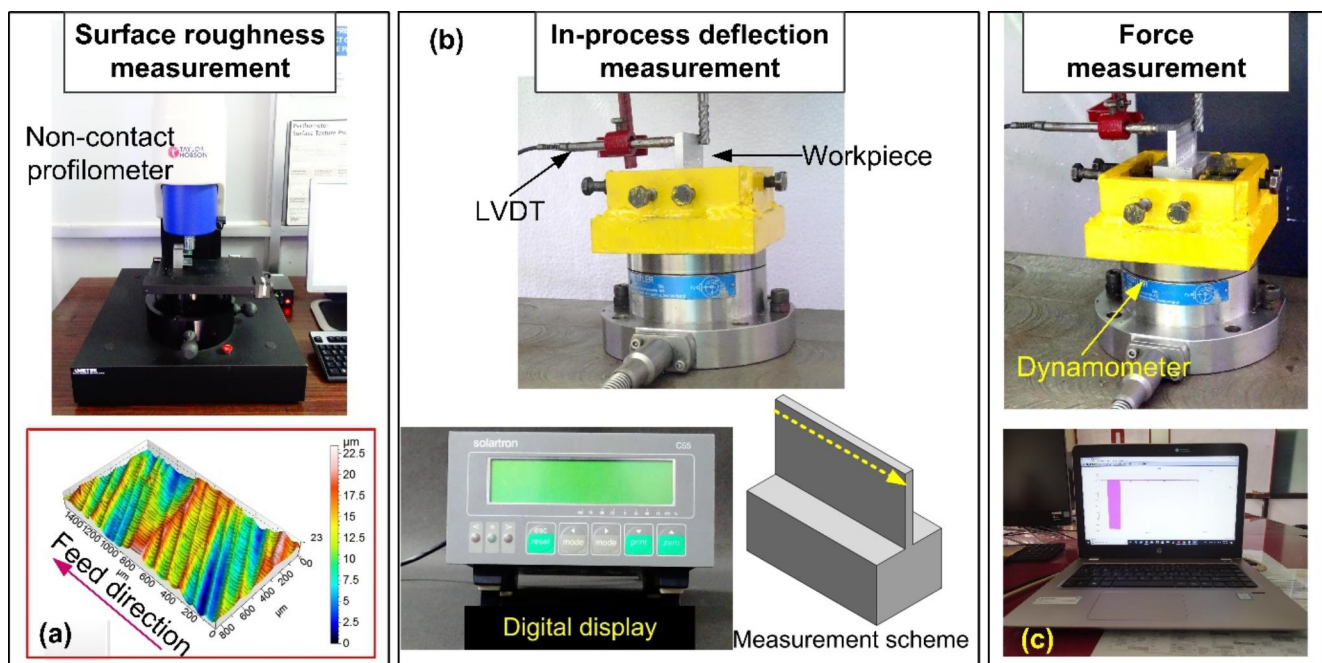

Fig. 3 Measurement of (a) Surface roughness, (b) In-process deflection, (c) Cutting forces

the end user can select the suitable levels of process variables that help meet the desired target. Accordingly, it has been shown that NSGA-II can generate a wide range of Pareto-optimal solutions based on the chosen process variables [26, 27]. Therefore, the present study employed NSGA-II to determine the combination of process variables for optimum performance. The NSGA-II toolbox developed by Sastry [28], was run using MATLAB 11.0. It typically took about 5 min on an Intel i7 machine with 8 GB RAM. Additional details regarding the NSGA-II procedure can be found in [29].

3 Results and discussion

In the presented study, eighty-one experiments were conducted. The measured performance parameters are listed in Table 2.

3.1 Product quality analysis

The surface roughness dictates the wear resistance and fatigue strength of the machined component, whereas the in-process wall deflection can produce dimensionally inaccurate parts.

In thin-wall machining, both performance measures are considered important quality measures, especially when the finishing operation is concerned. Therefore, a product quality parameter Q_i was defined by using the weighted function of surface roughness and wall deflection. The product quality parameter Q_I is given by:

$$Q_i = \left(\frac{D_{f\max} - D_f}{D_{f\max} - D_{f\min}} w_1 \right) + \left(\frac{R_{a\max} - R_a}{R_{a\max} - R_{a\min}} w_2 \right) \quad (2)$$

where Q_i is the quality index ($0 \leq Q_i \leq 1$). A higher Q_i value indicates superior surface finish and dimensional accuracy. For rough cuts, the index values are lower. The variables $D_{f\min}$, $D_{f\max}$, $R_{a\min}$, and $R_{a\max}$ symbolize the minimum and maximum magnitude of wall deflection and surface roughness, respectively. The terms w_1 and w_2 represent the weights assigned to the two quality parameters. In thin-wall machining operation, both the surface roughness and wall deflection have been considered equally important; therefore, an equal weightage was provided by choosing a value of 0.5. The Q_i also indicates the readiness of the selected process parameters for the finish machining of thin-wall parts when surface finish and dimensional accuracy are of utmost importance.

Table 3 lists the ANOVA for Q_i. Accordingly, it can be observed that the main effect factors d_i, f_z, a_d, r_d, the interaction of d_i with a_d, d_i with f_z, and a_d with r_d wit are significant

model terms. A high coefficient of determination (R^2) value of 93.67% implied that the model was significant. Further, adjusted-R^2 of 92.94% and predicted-R^2 of 91.89% were in reasonable agreement, indicating the model's adequacy. An adequate precision ratio of 45.33 showed an adequate S/N ratio (S/N > 4 is desirable). The normal probability plot, as seen in Fig. 4(a), verifies the normality test. Moreover, the distribution of the actual and predicted values along a straight-line signalled model satisfaction (see Fig. 4(b)).

The quadratic model of the response equation after eliminating the non-significant terms is given by,

$$Q_i = 0.7733 + 0.1491 \cdot d_i - 7.0811 \cdot f_z - 0.0391 \cdot a_d - 0.0912 \cdot r_d \\ + 0.2612 \cdot d_i \cdot f_z - 0.0154 \cdot a_d \cdot r_d - 0.0087 \cdot d_i \cdot d_i + 0.0013 \cdot a_d \cdot a_d \quad (3)$$

The main effect plots shown in Fig. 5 help visualize the influence of the process variables on Q_i. The plot which has the highest slope has the most significant impact on Q_i. Accordingly, d_i and r_d strongly influence Q_i, followed by f_z and a_d. Further observation revealed that Q_i increased as the d_i increased from 4 to 8 mm, but a drop was noted when a tool with larger d_i (16 mm) was used. Smaller diameter tools of 4 mm underwent deformation resulting in tool deflection and inferior surface finish due to chatter. However, with an 8 mm diameter tool, the machining process stabilized due to the higher rigidity of the tool. As a result, the Q_i improved, indicating a reduction in surface roughness and deflection. Further increase in the tool size to 12 mm, lowered the Q_i due to the intermittent nature of cutting forces. Higher intermittent cutting forces resulted in large in-process deflection and lowered the surface finish. The Q_i decreased linearly as f_z, a_d, and r_d decreased. Lower chip load at lower f_z condition (0.02 mm/z) generated lower cutting forces. As a result, in-process deflection and surface roughness was maintained at a minimum. However, as the f_z increased to 0.04–0.06 mm/z, the chip load increased, thus increasing the magnitude of the cutting force. Additionally, the adherence of chip material to the tool at higher f_z resulted in interrupted cutting, thereby increasing the surface roughness and wall deflection. The quality index Q_i also reduced at higher a_d, and r_d. The length and width of the work tool contact increased when the machining was carried out, maintaining a_d at 24 mm and r_d at 1.25 mm. This increased the cutting load and promoted uneven material removal and wall deflection. However, lower axial depth of cut (8 mm) and width of cut (0.3125 mm) results in stable cutting. As a result, a high surface finish with better dimensional accuracy was obtained. Additionally, the 3D response surfaces corresponding to ANOVA analysis were constructed as seen in Fig. 6. Q_i increased with the increase in d_i. But the further increase in d_i lowered the quality. Also, higher quality thin-wall can be produced by employing smaller f_z values. On

Table 2 Measured experimental results

Sl. No.	d_i	f_z	a_d	r_d	P_y	P_C	Q_i
	(mm)	(mm/z)	(mm)	(mm)	(mm³/min)	(W)	
1	12	0.06	8	0.3125	1119.4	139.48	0.779
2	12	0.02	8	0.3125	426.231	112.28	0.929
3	12	0.04	12	0.625	2063.11	235.51	0.717
4	12	0.02	12	0.625	1093.8	204.48	0.801
5	8	0.06	24	0.3125	3692.09	195.56	0.789
6	8	0.06	8	1.25	4854.06	217.67	0.595
7	8	0.02	8	1.25	1855.67	114.25	0.799
8	4	0.06	8	0.3125	1340.69	117.31	0.636
9	4	0.02	8	1.25	2057.01	81.11	0.634
10	8	0.02	12	1.25	2785.87	163.54	0.708
11	12	0.04	8	0.3125	795.88	122.46	0.815
12	12	0.06	24	0.3125	3396.98	504.59	0.669
13	12	0.02	8	1.25	1693.04	220.40	0.659
14	12	0.04	12	1.25	4753.03	377.12	0.527
15	12	0.04	24	0.625	4148.59	329.30	0.690
16	8	0.02	24	1.25	5585.98	235.21	0.624
17	4	0.04	24	1.25	*	*	*
18	12	0.02	24	1.25	5101.7	614.99	0.476
19	12	0.02	12	0.3125	640.06	136.28	0.868
20	8	0.04	24	0.625	4690.37	208.79	0.745
21	4	0.06	8	0.625	2528.09	135.48	0.534
22	4	0.02	24	1.25	6181.82	170.95	0.338
23	8	0.04	24	0.3125	2623.46	148.39	0.847
24	4	0.06	24	0.3125	4039.07	123.74	0.532
25	4	0.06	12	0.3125	2013.16	122.40	0.527
26	4	0.02	8	0.625	964.691	88.02	0.760
27	4	0.02	12	1.25	3086.54	107.96	0.503
28	12	0.06	8	1.25	4447.67	299.32	0.608
29	4	0.04	8	0.3125	957.447	104.90	0.698
30	8	0.04	12	0.3125	1305.91	86.63	0.849
31	4	0.02	8	0.3125	515.429	70.30	0.834
32	8	0.02	24	0.625	2492.67	129.72	0.869
33	12	0.04	12	0.3125	1196.06	183.34	0.731
34	4	0.04	8	0.625	1799.15	125.63	0.621
35	8	0.06	8	0.625	2194.49	99.47	0.713
36	12	0.06	8	0.625	1946.57	176.32	0.733
37	12	0.06	24	0.625	5902.78	593.80	0.635
38	12	0.02	24	0.3125	1284.42	244.71	0.842
39	4	0.02	12	0.3125	773.509	80.045	0.752
40	4	0.06	12	0.625	3796.53	145.94	0.341
41	4	0.02	24	0.625	2898.83	102.47	0.553
42	4	0.04	12	0.625	2701.27	133.51	0.418
43	4	0.04	24	0.3125	2882.44	119.18	0.632
44	12	0.06	24	1.25	13515.9	1049.16	0.238
45	12	0.02	8	0.625	728.571	138.97	0.859
46	8	0.02	12	0.3125	700.678	65.49	0.933
47	8	0.06	24	1.25	14683.3	505.15	0.265
48	8	0.02	8	0.625	828.281	59.69	0.934
49	12	0.04	8	1.25	3161.81	267.37	0.615
50	4	0.04	8	1.25	3821.18	109.93	0.558
51	8	0.02	24	0.3125	1404.7	99.71	0.954
52	8	0.06	12	0.3125	1834.53	117.71	0.783
53	12	0.04	24	0.3125	2407.17	408.18	0.730

Table 2 (continued)

Sl. No.	d_i (mm)	f_z (mm/z)	a_d (mm)	r_d (mm)	P_y (mm³/min)	P_C (W)	Q_i
54	4	0.02	12	0.625	1447.77	90.72	0.539
55	8	0.04	24	1.25	10436.6	391.94	0.396
56	4	0.02	24	0.3125	1549.21	82.01	0.768
57	8	0.04	12	0.625	2334.45	122.92	0.760
58	4	0.06	24	0.625	7619.52	153.99	0.350
59	8	0.02	8	0.3125	466.691	38.59	0.988
60	4	0.04	24	0.625	5414.01	151.42	0.437
61	4	0.06	8	1.25	5351.52	125.44	0.379
62	8	0.06	24	0.625	6640.63	275.76	0.679
63	12	0.06	12	1.25	6692.91	444.32	0.489
64	8	0.06	8	0.3125	1220.1	71.19	0.824
65	12	0.02	12	1.25	2542.37	305.00	0.585
66	4	0.06	12	1.25	*	*	*
67	12	0.06	12	0.625	2927.67	277.44	0.661
68	4	0.04	12	0.3125	1437.43	110.99	0.602
69	12	0.04	8	0.625	1372.69	166.39	0.757
70	12	0.04	24	1.25	9568.48	985.51	0.289
71	8	0.04	8	0.3125	869.516	60.07	0.898
72	8	0.04	8	0.625	1553.93	93.03	0.786
73	4	0.04	12	1.25	5736.78	143.52	0.461
74	12	0.02	24	0.625	2193.86	308.06	0.793
75	8	0.02	12	0.625	1243.5	92.90	0.872
76	8	0.06	12	0.625	3298.84	152.88	0.628
77	8	0.06	12	1.25	7299.62	310.31	0.383
78	4	0.06	24	1.25	*	*	*
79	8	0.04	12	1.25	5193.48	227.31	0.552
80	8	0.04	8	1.25	3456.85	165.43	0.665
81	12	0.06	12	0.3125	1683.54	185.53	0.692

*Unable to acquire data due to tool failure

Table 3 ANOVA for Q_i

Source	Sum of Squares	DOF	Mean Square	F-value	P-value	% Contribution
Model	2.25	8	0.2816	127.63	< 0.0001	
d_i	0.3096	1	0.3096	140.30	< 0.0001	10.65
f_z	0.5129	1	μ129	232.41	< 0.0001	17.64
a_d	0.3474	1	0.3474	157.44	< 0.0001	11.95
r_d	1.20	1	1.20	541.62	< 0.0001	41.27
$d_i * f_z$	0.0146	1	0.0146	6.63	0.0122	0.50
$a_d * r_d$	0.1204	1	0.1204	54.56	< 0.0001	4.14
d_i^2	0.3430	1	0.3430	155.44	< 0.0001	11.80
a_d^2	0.0599	1	0.0599	27.15	< 0.0001	2.06
Residual	0.1523	69	0.0022			
Cor. Total	2.41	77				

the other hand, a combination of lower a_d and r_d produced better quality parts.

3.2 Process productivity analysis

The accomplishment of high productivity and superior product quality is of importance during thin-wall machining. Therefore, the influence of process variables on productivity was analyzed. The productivity of the process (P_y) was estimated by considering the machining time t_m (s) and the volume of material removed V_m (mm³).
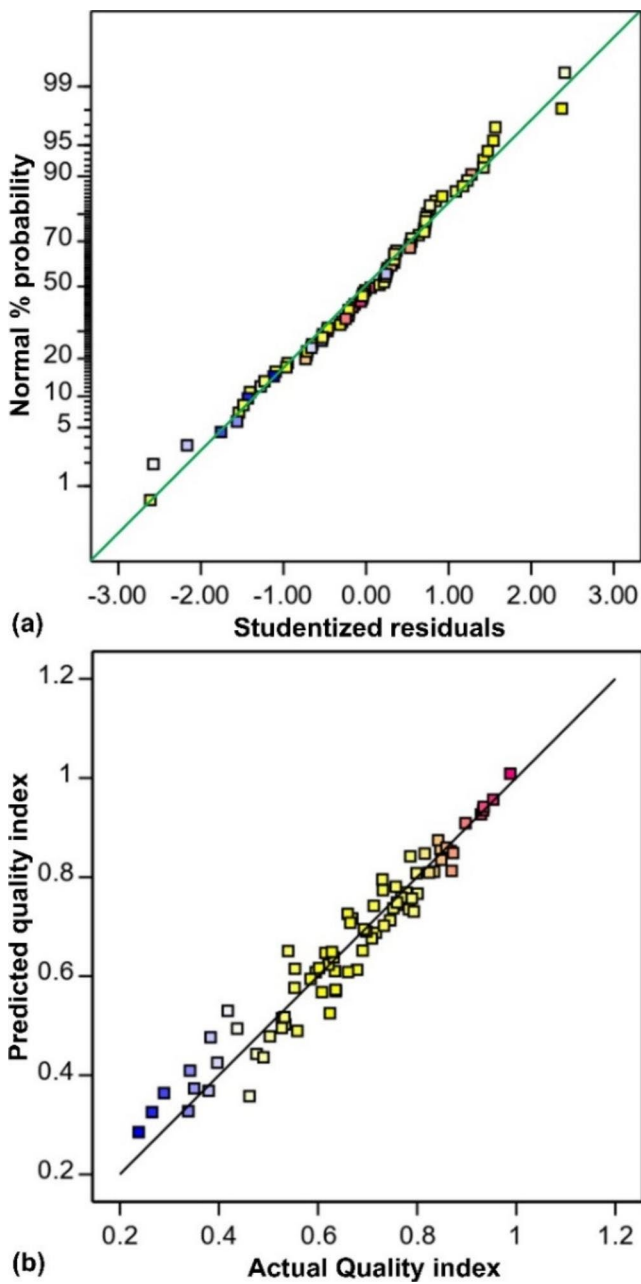
$$P_y = \frac{V_m}{t_m} \tag{4}$$

Fig. 4 (a) Normal probability plot of studentized residuals, (b) Plot of actual vs. predicted Q_i

The results of ANOVA for P_y are provided in Table 4. All four main factors and some of the interaction effects were found to be significant. Moreover, the R^2 of 98.23%, Predicted-R^2 of 97.45%, and adjusted-R^2 values of 98.05% indicated the significance of the model. Additionally, an adequate precision ratio of 102.25 suggests good response prediction accuracy. A normally distributed residuals (see Fig. 7(a)) also indicate the satisfactory performance of the developed model. Also, a strong correlation between the predicted and actual results suggests the accuracy of the
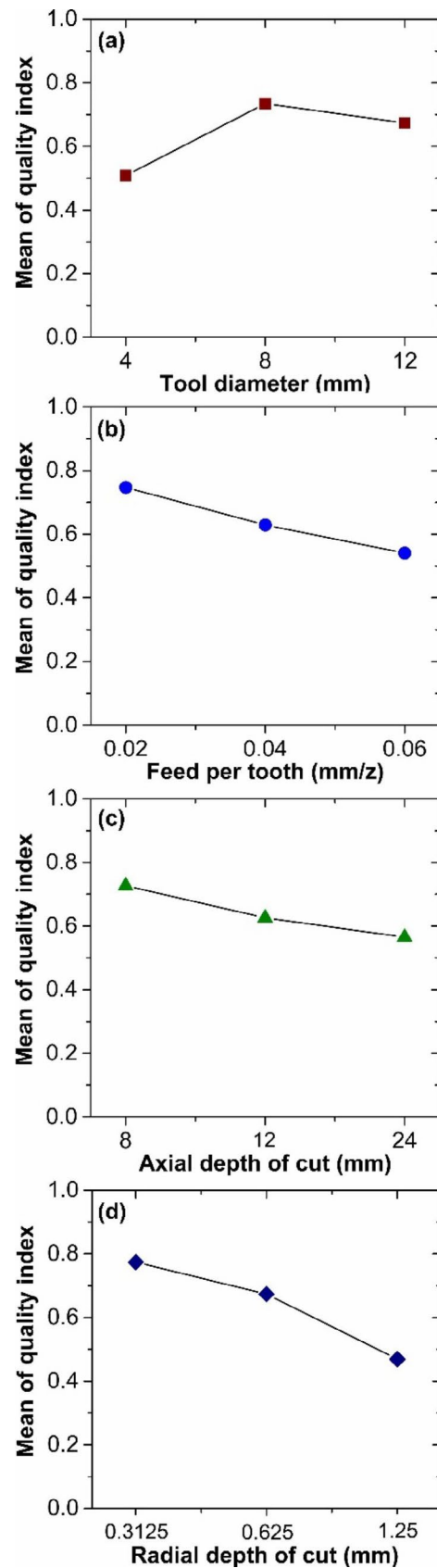
Fig. 5 Main effect plots for Q_i
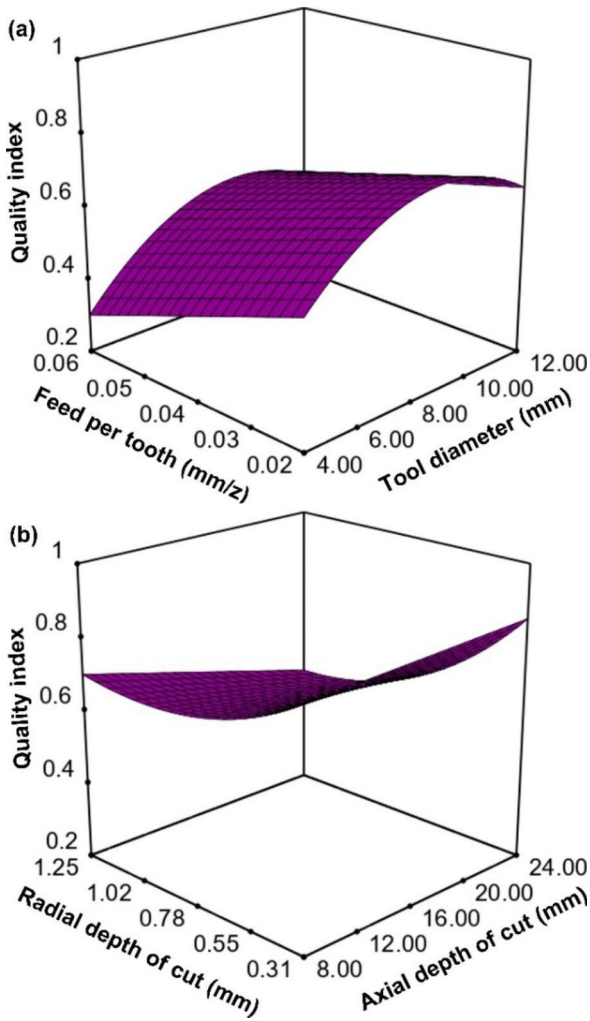
Fig. 6 3D contour plots of Q_i showing the interaction between (a) d_i and f_z, (b) d_i and a_d, (c) d_i and r_d, (d) f_z and a_d, (e) f_z and r_d, (f) a_d and r_d

Fig. 7 (a) Normal probability plot of studentized residuals; (b) Plot of actual vs. predicted P_y

developed model (see Fig. 7(b)). The response equation considering significant factors is given as:

$$P_y = 3340.84 - 71.54 \cdot d_i - 72366.74 \cdot f_z - 196.27 \cdot a_d - 3873.53 \cdot r_d \\ + 5019.94 \cdot f_z \cdot a_d + 1.0336e^{+5} \cdot f_z \cdot r_d + 316.36 \cdot a_d \cdot r_d \quad (5)$$
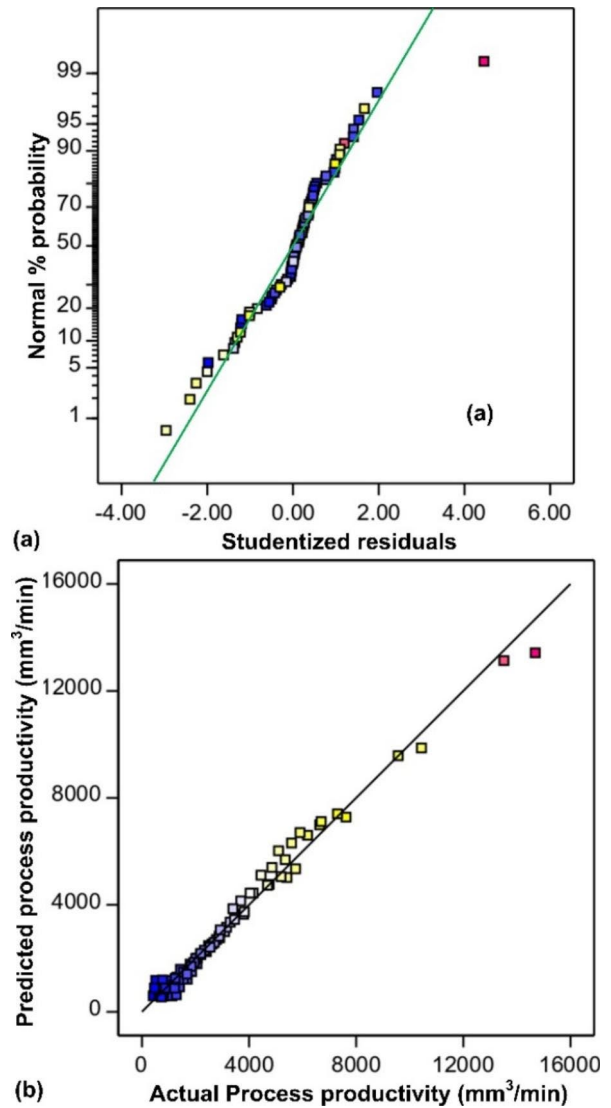
Figure 8 illustrates the main effect plot for P_y. P_y increased linearly with the increase in f_z, a_d, and r_d. However, an increase in d_i decreased the P_y marginally. Further, r_d and a_d had a more significant effect on P_y followed by f_z. At a lower

Table 4 ANOVA for P_y

| Source	Sum of Squares	DOF	Mean Square	F-value	P-value	% Contribution
Model	5.830E+08	7	8.329E+07	553.66	<0.0001	
d_i	4.096E+06	1	4.096E+06	27.23	<0.0001	0.54
f_z	1.492E+08	1	1.492E+08	991.81	<0.0001	19.30
a_d	2.140E+08	1	2.140E+08	1422.45	<0.0001	27.70
r_d	2.983E+08	1	2.983E+08	1982.74	<0.0001	38.60
$f_z * a_d$	2.405E+07	1	2.405E+07	159.89	<0.0001	3.11
$f_z * r_d$	3.221E+07	1	3.221E+07	214.13	<0.0001	4.15
$a_d * r_d$	5.099E+07	1	5.099E+07	338.98	<0.0001	6.60
Residual	1.053E+07	70	1.504E+05			
Cor. Total	5.935E+08	77				
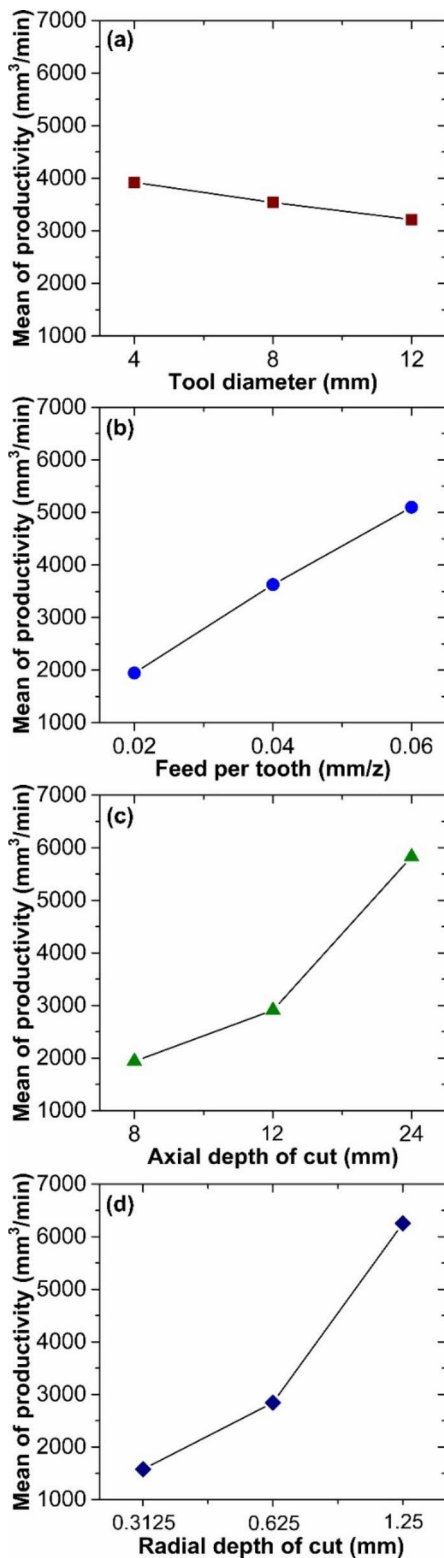
Fig. 8 Main effect plots for P_y

f_z (0.02 mm/z), the traverse speed of the tool will be slower. As a result, productivity suffers. However, as f_z increased to 0.06 mm/z, the tool traverse time reduced, which aided in improving the material removal rate and thus the P_y. The increase in P_y, with r_d and a_d can be linked to the cutter immersion and contact length. When a_d and r_d were maintained at 8 mm and 0.3125 mm, respectively, the contact length and cutter immersion remained smaller. This resulted in a lower material removal rate. However, with the increase in r_d and a_d to 1.25 and 24 mm, the cutter immersion and contact length increased, thus enhancing P_y. The effect of d_i on P_y showed an opposite trend compared to other process variables. P_y reduced as d_i increased. The increase in the ramp-on and ramp-off distances increased with d_i. As a result, the tool travel time increased, thereby decreasing P_y. Moreover, d_i was noted to have the most negligible influence on P_y. Figure 9(a) presents the effect of interaction between f_z and a_d on P_y, while Fig. 9(b) displays the interaction between f_z and r_d and its influence on P_y. Additionally, Fig. 9(c) illustrates the effect of interaction between a_d and r_d on P_y. The interaction plots show that higher P_y can be obtained by combining higher f_z and a_d, higher f_z, and r_d, or the combination of higher a_d and r_d.

3.3 Cutting power analysis

Power consumption is an indispensable part of the machining process, directly influencing the production cost and environmental pollution [17]. In the metal cutting process, the generated machining forces can estimate the cutting power (P_c). In the end milling operation, P_c is resolved into two components: the machining power of the spindle P_m power of feed motion P_f. Therefore, P_c is given by:

$$P_c = P_m + P_f \qquad (6)$$

where P_m is determined using,

$$P_m = \frac{F_x \pi n_s d_i}{60,000} \qquad (7)$$

and P_f is calculated by,

$$P_f = \frac{F_y n_s f_z}{60,000} \qquad (8)$$

Here F_x and F_y represent the cutting force and feed force components.

Table 5 depicts the ANOVA results for P_c. As noted, all four main factors and some of the interaction effects were found to be significant. Moreover, the R^2 of 93.17%, Predicted-R^2 of 89.42%, and adjusted-R^2 values of 92.03%
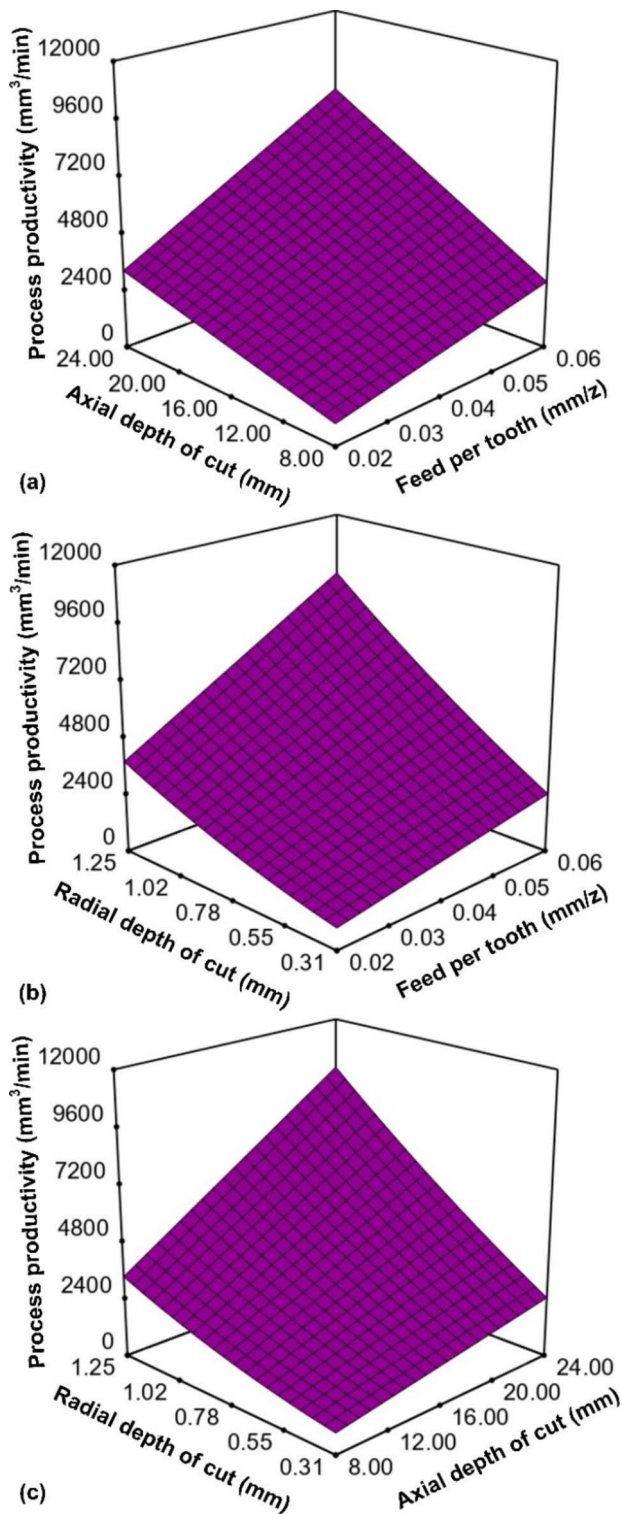
Fig. 9 3D contour plots of P_y showing the interaction between (a) f_z and a_d, (b) f_z and r_d, (c) a_d and r_d

indicated the significance of the model. An adequate precision ratio of 45.51 suggests good response prediction accuracy. A normally distributed residuals (see Fig. 10(a)) also indicate the satisfactory performance of the developed model. Also, a strong correlation between the predicted and actual results suggests the accuracy of the developed model (see Fig. 10(b)). The regression model for P_c after eliminating the non-significant terms is given by:

$$
\begin{aligned}
P_c = {} & 743.96 - 113.21 \cdot d_i - 4766.09 \cdot f_z - 28.16 \cdot a_d - 374.14 \cdot r_d \\
& + 269.47 \cdot d_i \cdot f_z + 2.49 \cdot d_i \cdot a_d + 29.48 \cdot d_i \cdot r_d + 234.44 \cdot f_z \cdot a_d \\
& + 2597.69 \cdot f_z \cdot r_d + 15.09 \cdot a_d \cdot r_d + 4.34 \cdot d_i \cdot d_i
\end{aligned} \tag{9}
$$

Figure 11 illustrates the main effect plot for P_c. P_c increased as d_i, f_z, a_d, and r_d increased. In a machining operation, P_c is a function of cutting force. Any increase in the magnitude of cutting force increases power consumption. When a lower f_z of 0.02 mm/z was considered, a smaller magnitude cutting force was generated due to smaller cutter contact with the work material. However, the cutter tool contact length increased with the increase in f_z to 0.06 mm/z. The resulting increase in the cutting force increased P_c. On similar lines, the P_c increased with the size of the tool used. The selection of a_d, and r_d also influenced the P_c. As the axial depth of cut increased from 8 to 24 mm, the engagement length between the cutting edge and the workpiece increased. This increased the magnitude of cutting force and thus the P_c. Similarly, as r_d increased from 0.3125 to 1.25 mm, the cutter immersion and hence the width of the cut increased. The resulting increase in the cutting forces increased P_c. Figure 12(a–f) depict the response surface plotted for P_c. From Fig. 12(a), P_c increased with the increase in d_i and f_z. Figure 12(b) shows that P_c increased with the rise in d_i and a_d. Similarly, P_c increased with d_i and r_d as seen in Fig. 12(c). The response plot shown in Fig. 12(d) indicated that Pc increased linearly with f_z and a_d. Also, as noted from Fig. 12(e, f), P_c increased with the combination of higher f_z and r_d, or higher a_d, and r_d.

3.4 Multi-objective optimization

Utilization of optimized process parameters can help in enhancing the thin-wall machining performance. Superior performance can be achieved by maximizing Q_i, P_y, and minimizing P_c. However, the defined objectives were contradictory and depended extensively on the machining requirement, i.e., roughing or finishing. Therefore, multi-objective optimization is essential to analyze the conflicting performance variables. Figure 13 summarizes the framework for optimizing the thin-wall machining operation.

According, the objective function was formulated as:

Table 5 ANOVA for P_c

Source	Sum of Squares	DOF	Mean Square	F-value	P-value	% Contribution
Model	2.329E+06	11	2.117E+05	81.84	<0.0001	
d_i	6.141E+05	1	6.141E+05	237.39	<0.0001	25.77
f_z	1.863E+05	1	1.863E+05	72.03	<0.0001	7.82
a_d	5.521E+05	1	5.521E+05	213.44	<0.0001	23.17
r_d	4.320E+05	1	4.320E+05	167.02	<0.0001	18.13
d_i*f_z	15255.61	1	15255.61	5.90	0.0179	0.64
d_i*a_d	2.201E+05	1	2.201E+05	85.10	<0.0001	9.23
d_i*r_d	95232.04	1	95232.04	36.82	<0.0001	4.00
f_z*a_d	52062.48	1	52062.48	20.13	<0.0001	2.18
f_z*r_d	19856.21	1	19856.21	7.68	0.0073	0.83
a_d*r_d	1.126E+05	1	1.126E+05	43.53	<0.0001	4.72
d_i^2	83726.99	1	83726.99	32.37	<0.0001	3.51
Residual	9.472E+06	69	1.373E+05			
Cor. Total	5.935E+08	77				
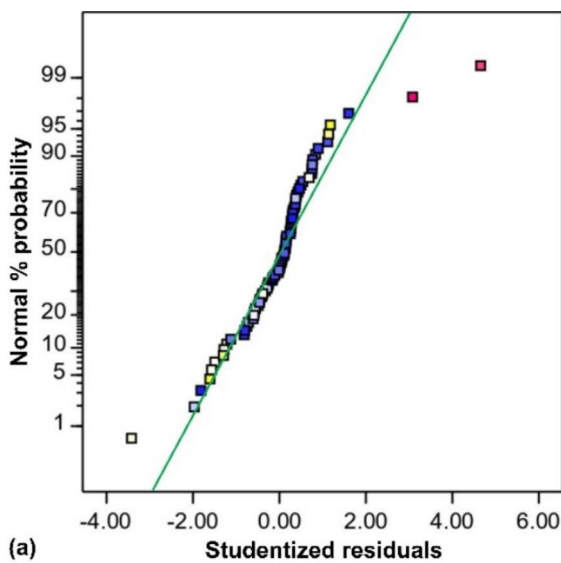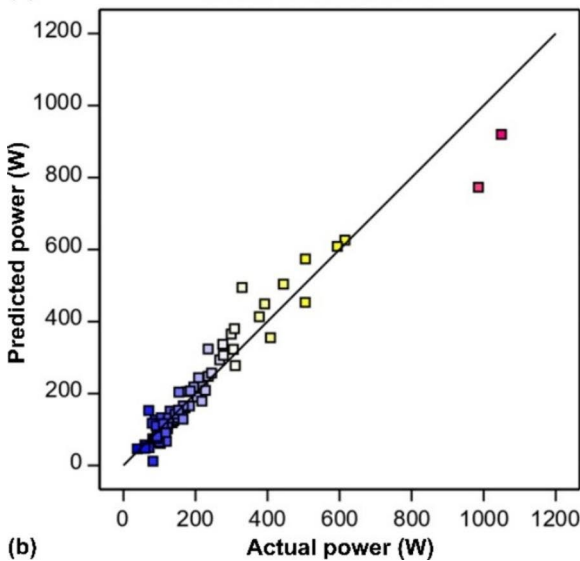
Fig. 10 (a) Normal probability plot of studentized residuals; (b) Plot of actual vs. predicted P_c

$$\max f(X) = \max\left(Q_i, \ P_y, \ \frac{1}{P_c}\right)^{\mathrm{T}} \quad (10)$$

Subjected to operation constraints,

$$\left.\begin{array}{l} d_{i\min} \leqslant d_i \leqslant d_{i\max} \\ f_{z\min} \leqslant f_z \leqslant f_{z\max} \\ a_{d\min} \leqslant a_d \leqslant a_{d\max} \\ r_{d\min} \leqslant r_d \leqslant r_{d\max} \end{array}\right\} \quad (11)$$

Here, $d_{imin}, d_{imax}, f_{zmin}, f_{zmax}, a_{dmax}$ and a_{dmin} are the minimum and maximum values of tool diameter, feed per tooth, maximum axial depth of cut, and radial depth of cut, respectively. In the present study, optimization objectives were required to satisfy the following criteria:

$$\left.\begin{array}{l} P_y > 13,000 \ ^{\mathrm{m}^3}/_{\min}(\text{Roughning operation}) \\ P_c < 650 \ \text{W (Roughning operation)} \\ Q_i < \ 00.8 \ (\text{Finishing operation}) \\ R_a < 0.6 \ \mu\text{m (Finishing operation)} \\ D_f < 0.075 \ \text{mm (Finishing operation)} \end{array}\right\} \quad (12)$$

Table 6 lists the NSGA-II algorithm parameter settings used in the present study. Figure 14 illustrates the developed 3-D Pareto front, which can investigate the trade-offs between different objective functions. The figure shows two regions, 'A' and 'B', appropriate to satisfy the two machining conditions viz. roughing operation and finishing operation. Here the solutions described in region 'A' can help boost productivity but at the expense of product quality and power consumption. On the contrary, machining with the solutions enclosed in region 'B' can produce dimensionally accurate thin-walls with a high-quality surface finish.
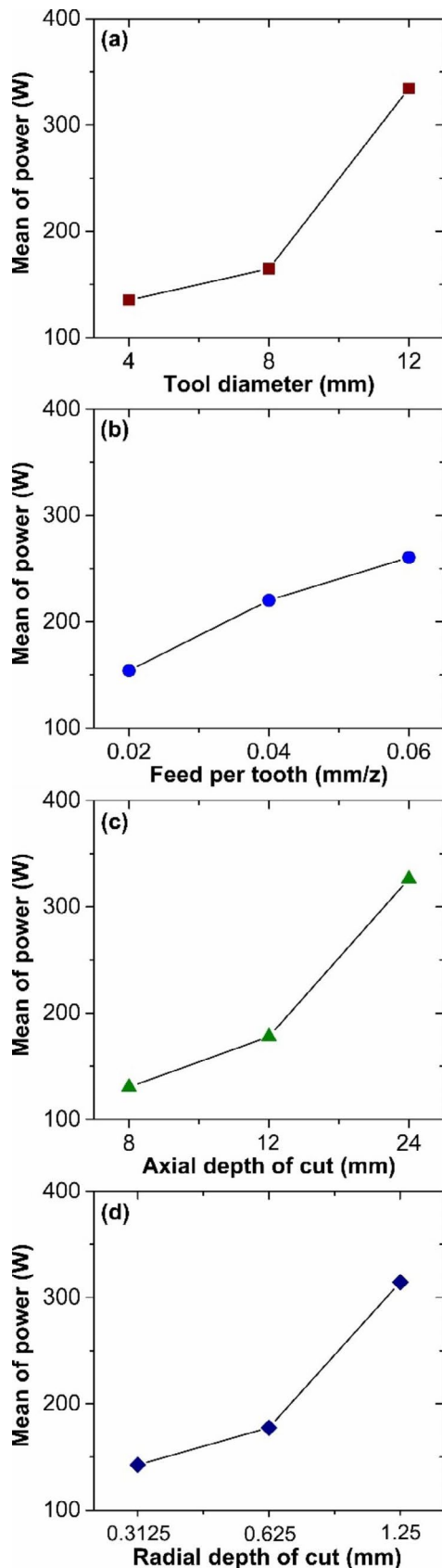
Fig. 11 Main effect plots for P_c

3.4.1 Optimum parameters for roughing operation

Considering the requirement of large material removal volume, maximizing Py during the initial stages of machining is essential. Table 7 lists some of the optimal Pareto solutions for maximizing P_y. However, a few optimal process combinations (Sol. No. 1, 3, 9) were found unsuitable for maximizing P_y. Thin-wall machining using a 4 mm end mill was reported to be undesirable due to the severe chatter resulting from the employment of higher depth of cut conditions [25]. Therefore, after a careful review, a few Pareto solutions proposed in Table 7 (Sl. No. 2 and 5) were selected for validation. Table 8 lists the predicted and measured MRR values for the optimal process conditions. A comparison of the same revealed that the absolute average deviation in productivity is no more than 9%, thus verifying the accuracy of the predictive model. Moreover, a maximum material removal of 1215 mm³/min was reported by Qu et al. [20]. It has to be noted that there is a significant improvement in the magnitude of the material removal rate (14,683 mm³/min) as compared to the previous study.

3.4.2 Optimum parameters for finishing operation

The Pareto solutions that provide high Qi were considered optimal solutions for the finish machining of thin-wall parts. Table 9 lists some of the optimal process parameter combinations for maximizing the Qi. Table 10 exhibits a comparison between the predicted and measured responses based on the Pareto solutions. The measured responses closely match with the solutions predicted by the developed model. The selected process parameter combinations can reduce the surface roughness and the magnitude of wall deflection. Figure 15 exhibits the 3-D topographies of the machined surface obtained before and after optimization. It is noticed the surface finish improved significantly with the use of optimal process parameters. The selected optimum process parameter combinations present a roughness of 0.331 and 0.494 μm. The measured surface roughness is significantly better than the roughness observed by other researchers. In the case of Vukman et al. [30], the lowest surface roughness observed was around 0.5 μm while milling aluminum alloy. Similarly, upon optimization, surface roughness varying between 1.03 and 1.17 μm was measured by Qu et al. [20] while machining hardened die steel. Therefore, it can be concluded that the optimized process variables from the present study can produce a comparatively better surface finish.

Furthermore, the application of optimal process parameters helped considerably reduce the milling power (P_c). Additionally, the quality of the thin-wall considering the form error was also analyzed. As noted in Table 10,
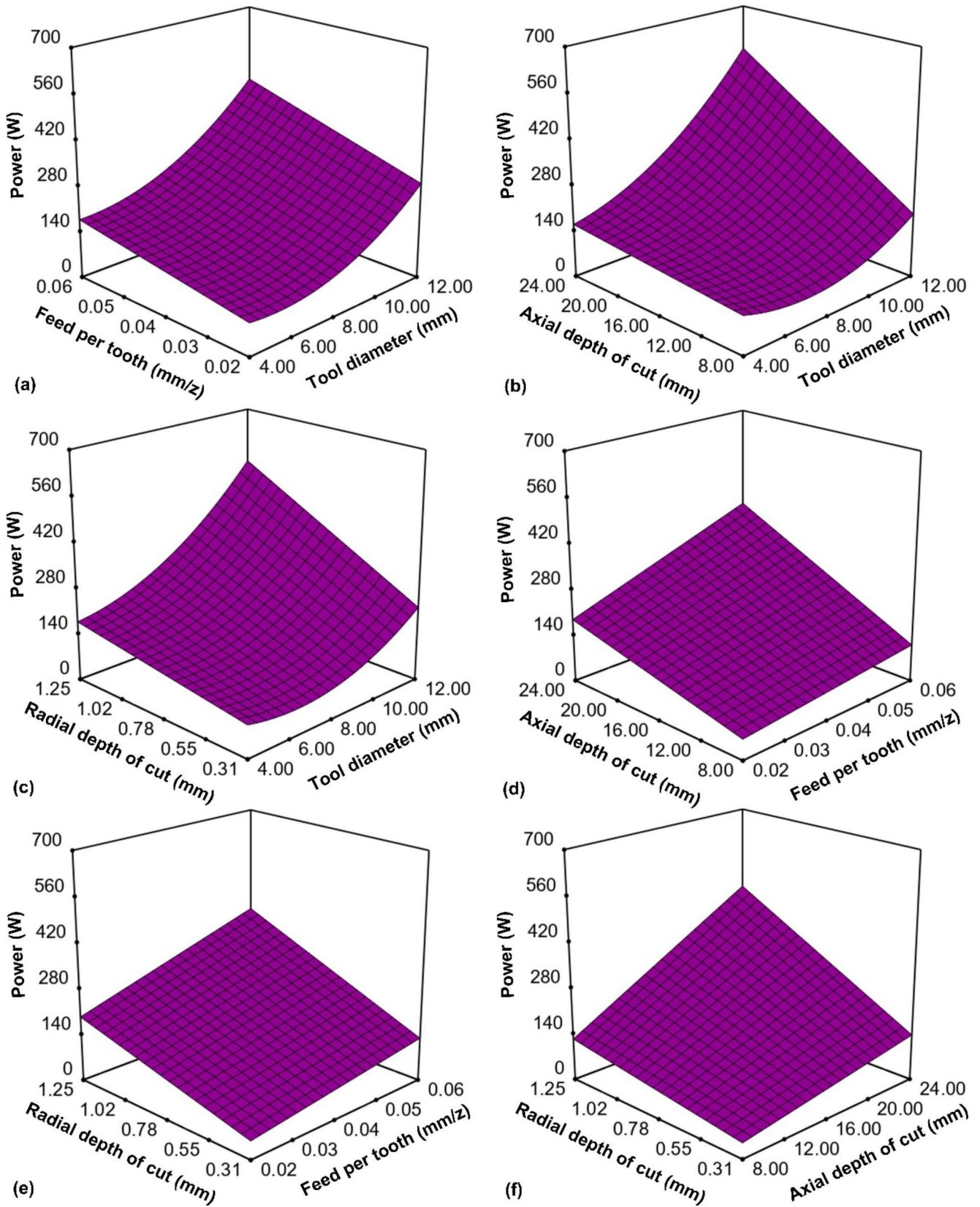
Fig. 12 3D contour plots of P_c showing the interaction between (a) d_i and f_z, (b) d_i and a_d, (c) d_i and r_d, (d) f_z and a_d, (e) f_z and r_d, (f) a_d and r_d

Fig. 13 Multi-objective optimization framework
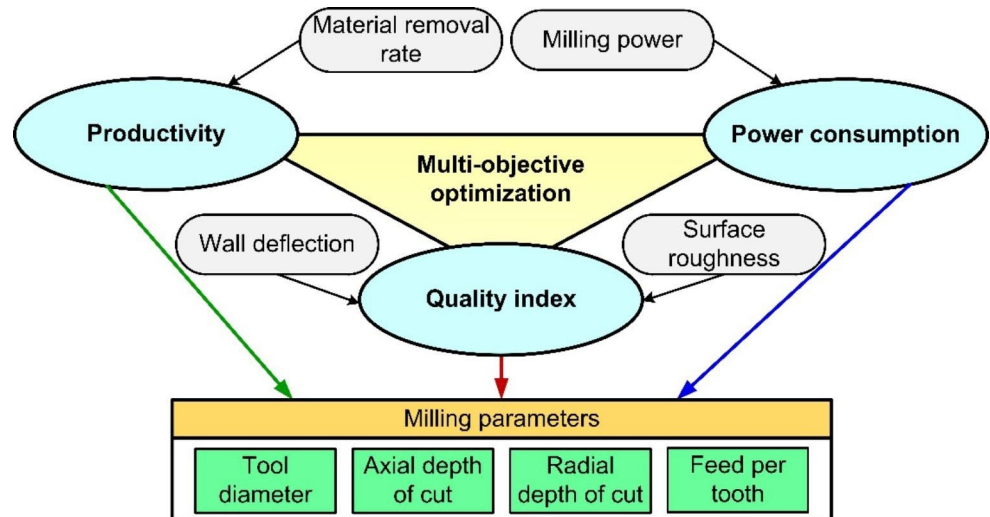
Table 6 NSGA-II parameters

Attribute		Value/condition
Population size		100
Tournament		Binary Tournament selection
Reproduction		0.8
Mutation		Constraint dependent
Crossover		Intermediate
Number of iterations		200
Mutation	Fraction	0.2
	Interval	20
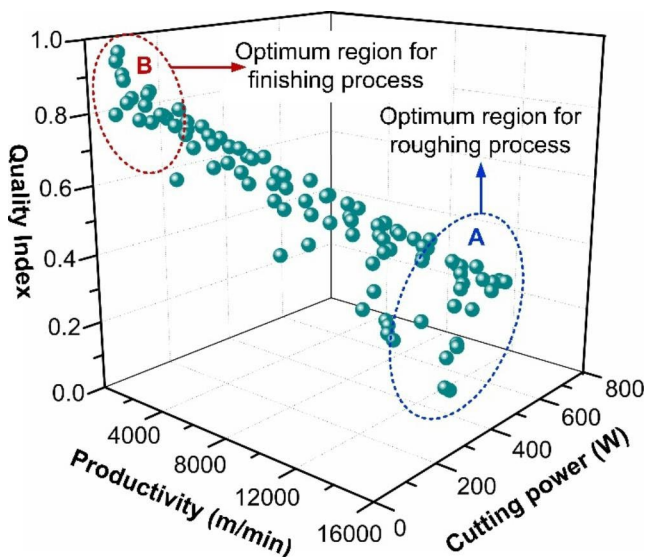
Fig. 14 3D plot of the Pareto-optimal solutions for Q_i, P_y and P_c

incorporating optimal process parameters lowered the average in-process wall deflection. Figure 16 presents the comparison between the deflection-induced form error. The incorporation of optimal process conditions significantly improves the dimensional accuracy of the thin-wall parts. The thickness of the wall at the free end was reduced to

1.283 and 1.298 mm from 1.991 mm. A few studies have measured the in-process wall deflection. According to work carried out by Izamshah et al. [31], the maximum recorded wall deflection was 0.12 mm. However, in the present study, the magnitude of wall deflection after optimization is noted to be 0.033 and 0.048 mm, respectively. The measured in-process deflection is significantly lowered than the value reported by other literature, thus affirming the capability of optimized process variables. The cutting power (P_c) needed to finish machine the thin-wall machining was analyzed. Machining thin-wall parts with the optimal process parameter combination lowered the P_c, as reported in Table 10. Further, a maximum deviation of 6% between the predicted and measured cutting power certified the predictive model's accuracy. Based on the investigation, the optimal combination denoted by the Pareto front can be recommended for energy-conscious machining of quality thin-wall parts.

3.4.3 Machining ultra-thin-walls using optimum parameters

The validity of the Pareto optimal solutions was evaluated further by carrying out the experiments on ultra-thin walls of 0.7 mm thickness. Figure 17 displays the 3-D topographies of the ultra-thin-wall surfaces machined using optimal conditions listed in Table 10. The thin-walls machined using the predicted optimal process parameter combination show an excellent surface finish, with the average surface roughness varying between 0.5 and 0.65 μm. Moreover, on inspection, the thickness of the wall at the free end was found to vary between 0.765 and 0.782 mm. These results further fortify the fact that the predicted optimal process parameters can be utilized to machine ultra-thin-wall parts using commercial low-medium duty CNC-VMC in real-life shop-floor conditions.

Table 7 Suggested combinations of optimum parameters for maximizing P_y

Sol. No.	Milling parameters				Response parameters		
	d_i (mm)	f_z (mm/z)	a_d (mm)	r_d (mm)	Q_i	P_c (W)	P_y (mm³/min)
1	4	0.0594	23.99	1.2442	0.093	372.96	13919.17
2	7	0.0594	23.94	1.2381	0.263	507.61	13409.05
3	4.9	0.0587	23.97	1.238	0.163	399.65	13588.75
4	5.4	0.0598	23.99	1.2389	0.187	427.9	13736.23
5	8.6	0.0589	23.86	1.2361	0.303	606.91	13036.97
6	5.5	0.0597	23.95	1.2384	0.194	430.96	13678.43
7	8.9	0.06	23.85	1.2379	0.301	636.87	13205.99
8	8.6	0.0581	23.81	1.2267	0.313	595.88	12767.72
9	4	0.06	24	1.2500	0.087	378.41	14098.5
10	8.2	0.0595	23.95	1.2447	0.289	588.8	13339.6

Table 8 Verification of the optimum conditions for roughing operation

Sl. No	Milling parameters					P_y (mm³/min)
	d_i (mm)	f_z (mm/z)	a_d (mm)	r_d (mm)		
1	9	0.06	24	1.25	Predicted	13402.59
	8	0.06	24	1.25	Measured	14683.30
					Deviation (%)	8.72
2	7	0.06	24	1.25	Predicted	13680.95
	8	0.06	24	1.25	Measured	14683.30
					Deviation (%)	6.28

Table 9 Suggested combinations of optimum parameters for maximizing Qi and minimizing P_y

Sl. No	Milling parameters				Response parameters		
	d_i (mm)	f_z (mm/z)	a_d (mm)	r_d (mm)	Q_i	P_c (W)	P_r (mm³/min)
1	8.9	0.02	8.22	0.3158	0.965	51.95	878.2777
2	8.9	0.0314	8.24	0.4887	0.889	56.42	1034.027
3	8.9	0.0202	8.25	0.4887	0.941	47.29	820.2631
4	7.3	0.0269	23.28	0.3757	0.852	89.01	1831.928
5	5.8	0.0234	23.18	0.4445	0.789	56.34	2006.509
6	6	0.0211	23.14	0.3887	0.834	44.71	1511.242
7	8.4	0.0265	9.07	0.4243	0.905	55.62	985.3546
8	4.8	0.0201	23.43	0.3181	0.803	24.98	1208.125
9	7.6	0.0267	23.02	0.3766	0.859	96.03	1779.879
10	8.9	0.0201	8.22	0.3158	0.965	51.98	878.3563

Table 10 Verification of the recommended optimum conditions for finishing operation

Sl. No	Milling parameters					Performance measures			
	d_i (mm)	f_z (mm/z)	a_d (mm)	r_d (mm)		R_a (μm)	D_f (mm)	Q_i	P_c (W)
1	8.9	0.02	8.22	0.316	Predicted	0.298	0.048	0.965	51.94
	8	0.02	8	0.3125	Measured	0.331	0.027	0.983	50.12
					Deviation (%)	9.85	43	1.18	3.5
2	8.9	0.031	8.24	0.489	Predicted	0.456	0.047	0.891	56.09
	8	0.03	8	0.5	Measured	0.484	0.034	0.89	59.47
					Deviation (%)	5.83	27.6	0.11	5.83

The predicted optimal process parameters were also used to machine curvilinear ultra-thin-walls of 0.7 mm thickness. The final reduction in thickness was obtained by machining the curvilinear thin-walls in convex mode (synclastic machining) and concave mode (anticlastic machining). Figure 18 exhibits the machined ultra-thin-walls along with the surface topographies of the machined surfaces. The predicted process parameters were able to machine curvilinear
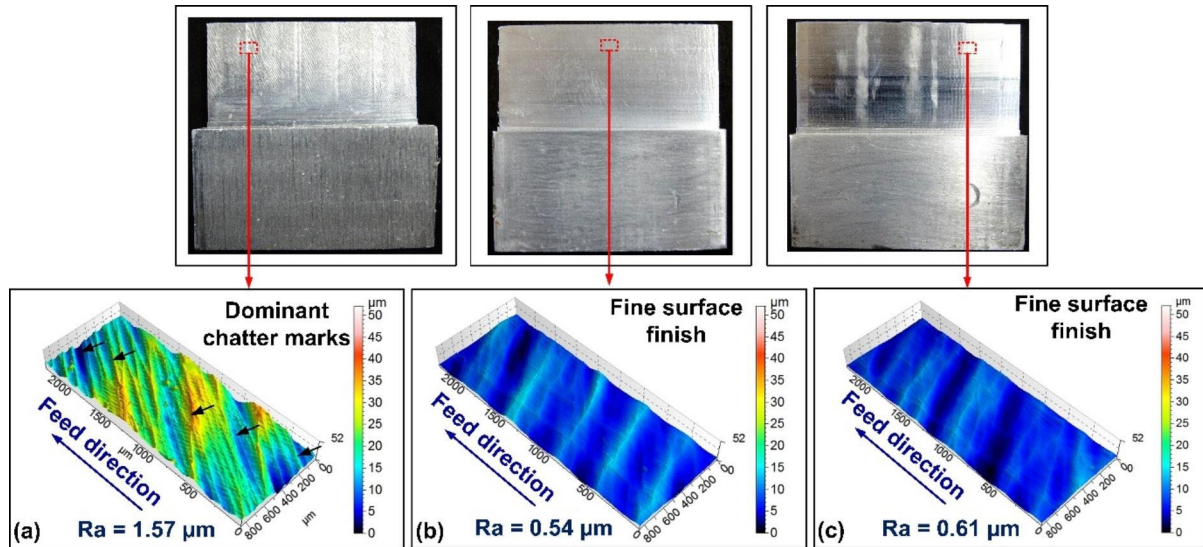
Fig. 15 Machined surface and 3-D surface topography for (a) Non-optimized process parameters; (b) Optimal condition-1 listed in Table 10; (c) Optimal condition-2 listed in Table 10

thin-walls with uniform thickness and excellent surface finish. On closer inspection, the curvilinear wall showed a better surface finish than open straight walls. The higher rigidity of the curvilinear walls helped reduce the in-situ wall deflection and improved the surface finish. Moreover, anticlastic machining resulted in more significant form errors than synclastic machining, as seen in Fig. 18. The occurrence is attributed to the larger magnitude of the milling force, as depicted in Table 11. However, the predicted optimal milling parameters were able to machine straight and curvilinear ultra-thin-walls with excellent surface finish and dimensional accuracy.

4 Conclusion

The influence of thin-wall milling parameters viz. tool diameter, feed per tooth, axial and radial depth of cut on productivity, and product quality and cutting power was analyzed. The statistical significance of the process variables on the three performance measures was assessed using ANOVA. The NSGA-II was employed to determine the optimal process parameters to enhance productivity and product quality while minimizing the cutting power. Based on the outcomes, the following conclusions have been formulated.

- The ANOVA results indicated that the selected input parameters significantly contributed to the thin-wall machining process. The quality and productivity were enhanced by milling with a smaller diameter tool and employing lower values of f_z, a_d, and r_d. An increment

in the process productivity was obtained at higher d_i, f_z, a_d, and r_d values.

- The correlation of P_c, P_y, and Q_i was established to explore the influence of d_i, f_z, a_d, and r_d. Based on the higher values of evaluating coefficients, the developed statistical models are recommended for predicting the response outputs.
- NSGA-II based optimization model was successful in generating optimal Pareto solutions for roughing and finishing operations. The optimized process parameters for roughing operation helped in maximizing the process productivity. At the same time, the Pareto solutions for finishing operation effectively improved energy efficiency and produced quality thin-wall parts. Improved surface finish with minimal deflection was obtained by milling with cutters of diameter 8 ~ 9 mm and maintaining the feed, axial, and radial depth at 0.02 mm/z, 8 mm, and 0.3125 mm, respectively.
- The results can be employed for milling Aluminum alloy thin-wall parts. The study provides a wide range of solutions for machinists and decision-makers who are involved in the production of thin-wall structures. The central findings provide effective solution for end milling open straight and curved thin-wall parts, especially when high productivity, product quality, and energy efficiency are mandated.
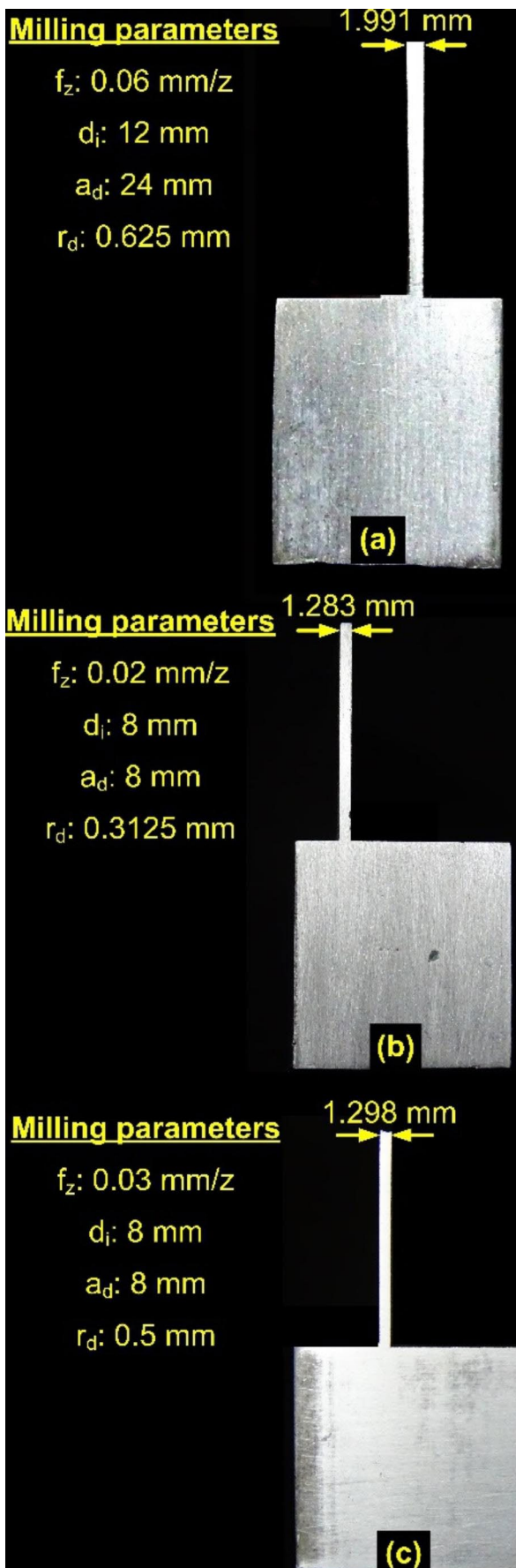
Fig. 16 Form error for (a) Non-optimized process parameters; (b) Optimal condition-1 listed in Table 10; (c) Optimal condition-2 listed in Table 10

Fig. 17 Surface finish and form error for (a) Optimal condition-1 listed in Table 10; (b) Optimal condition-2 listed in Table 10
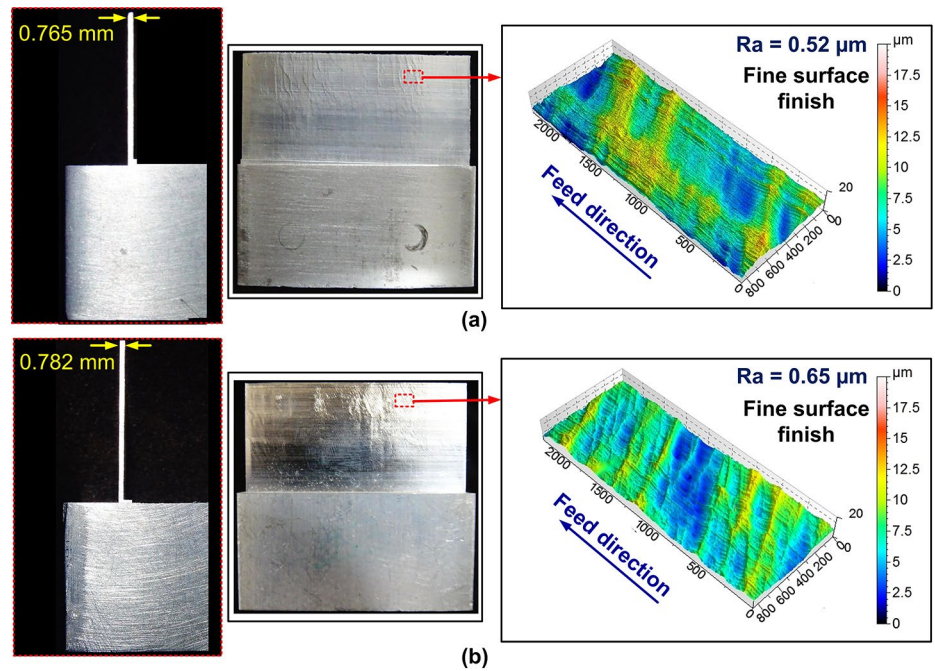

Fig. 18 Surface finish and form error while machining curvilinear thin-wall part (a) Concave surface, (b) Convex surface
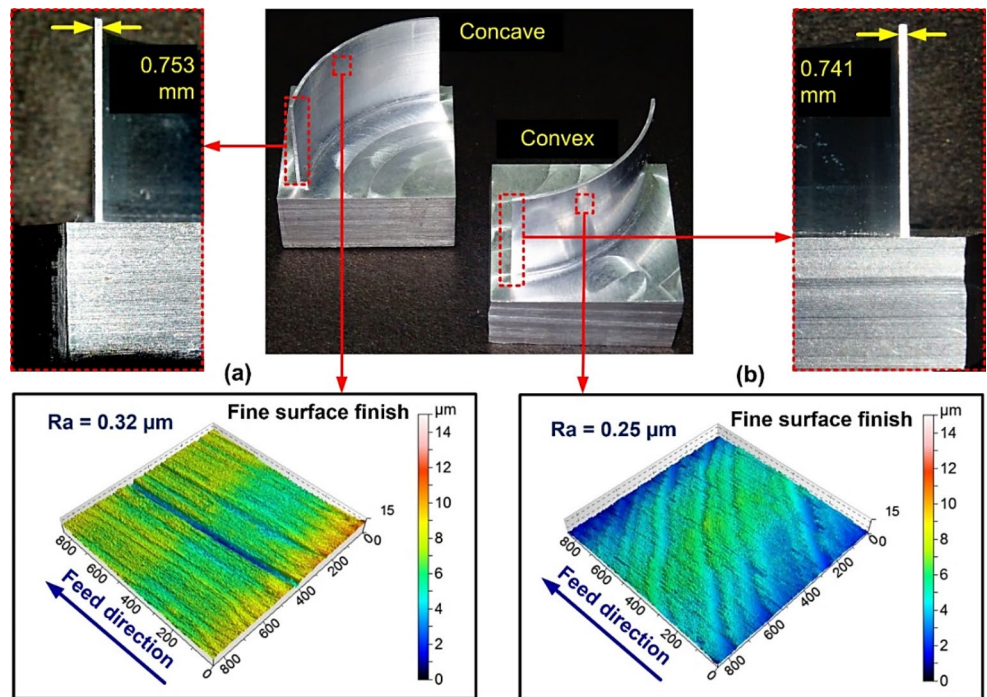

Table 11 Comparison of response parameters for curvilinear thin-walls

Geometry	Milling force F_r (N)	Surface roughness R_a (μm)	Wall deflection D_f (mm)
Concave	65.40	0.32	0.041
Convex	47.51	0.25	0.032

Declarations

Conflicts of interest/Competing interests Authors declare no conflict of interest.

Open Access This article is licensed under a Creative Commons Attribution 4.0 International License, which permits use, sharing, adaptation, distribution and reproduction in any medium or format, as long as you give appropriate credit to the original author(s) and the source, provide a link to the Creative Commons licence, and indicate if changes were made. The images or other third party material in this article are included in the article's Creative Commons licence, unless indicated otherwise in a credit line to the material. If material is not included in the article's Creative Commons licence and your intended use is not permitted by statutory regulation or exceeds the permitted use, you will need to obtain permission directly from the copyright holder. To view a copy of this licence, visit http://creativecommons.org/licenses/by/4.0/.

References

1. Del Sol, I., Rivero, A., López de Lacalle, L.N., Gamez, A.J.: Thin-Wall Machining of Light Alloys: A Review of Models and Industrial Approaches. *Materials* 12, (2019) (2012)
2. Zhang, Y., Zou, P., Li, B., Liang, S.: Study on optimized principles of process parameters for environmentally friendly machining austenitic stainless steel with high efficiency and little energy consumption. Int. J. Adv. Manuf. Technol. **79**, 89–99 (2015)
3. Rajeswari, B., Amirthagadeswaran, K.S.: Experimental investigation of machinability characteristics and multi-response optimization of end milling in aluminium composites using RSM based grey relational analysis. Measurement. **105**, 78–86 (2017)
4. Wojciechowski, S., Maruda, R.W., Krolczyk, G.M., Nieslony, P.: Application of signal to noise ratio and grey relational analysis to minimize forces and vibrations during precise ball end milling. Precis Eng. **51**, 582–596 (2018)
5. Pa, N.M.N., Sarhan, A.A.D., Abd Shukor, M.H.: Optimizing the cutting parameters for better surface quality in 2.5 D cutting utilizing titanium coated carbide ball end mill. Int. J. Precis Eng. Manuf. **13**, 2097–2102 (2012)
6. Ren, J., Zhou, J., Zeng, J.: Analysis and optimization of cutter geometric parameters for surface integrity in milling titanium alloy using a modified grey–Taguchi method. Proc. Inst. Mech. Eng. B J. Eng. Manu. 230, 2114–2128 (2016)
7. Tlhabadira, I., Daniyan, I.A., Machaka, R., Machio, C., Masu, L., VanStaden, L.R.: Modelling and optimization of surface roughness during AISI P20 milling process using Taguchi method. Int. J. Adv. Manuf. Technol. **102**, 3707–3718 (2019)
8. Sarıkaya, M., Yılmaz, V., Dilipak, H.: Modeling and multi-response optimization of milling characteristics based on Taguchi and gray relational analysis. Proc. Inst. Mech. Eng. B J. Eng. Manu. 230, 1049–1065 (2016)
9. Jomaa, W., Lévesque, J., Bocher, P., Divialle, A., Gakwaya, A.: Optimization study of dry peripheral milling process for improving aeronautical part integrity using Grey relational analysis. Int. J. Adv. Manuf. Technol. **91**, 931–942 (2017)
10. Karabulut, Å., Gökmen, U., Çinici, H.: Optimization of machining conditions for surface quality in milling AA7039-based metal matrix composites. Arab. J. Sci. Eng. **43**, 1071–1082 (2018)
11. Campatelli, G., Lorenzini, L., Scippa, A.: Optimization of process parameters using a response surface method for minimizing power consumption in the milling of carbon steel. J. Clean. Prod. **66**, 309–316 (2014)
12. Jang, D.Y., Jung, J., Seok, J.: Modeling and parameter optimization for cutting energy reduction in MQL milling process. Int. J. Precis Eng. Manuf. Technol. **3**, 5–12 (2016)
13. Zhang, H., Deng, Z., Fu, Y., Lv, L., Yan, C.: A process parameters optimization method of multi-pass dry milling for high efficiency, low energy and low carbon emissions. J. Clean. Prod. **148**, 174–184 (2017)
14. Ahmed, S.U., Arora, R.: Quality characteristics optimization in CNC end milling of A36 K02600 using Taguchi's approach coupled with artificial neural network and genetic algorithm. Int. J. Syst. Assur. Eng. Manag. **10**, 676–695 (2019)
15. Nguyen, T.T., Nguyen, T.A., Trinh, Q.H.: Optimization of milling parameters for energy savings and surface quality. Arab. J. Sci. Eng. **45**, 9111–9125 (2020)
16. Kar, T., Mandal, N.K., Singh, N.K.: Multi-response optimization and surface texture characterization for CNC milling of inconel 718 alloy. Arab. J. Sci. Eng. **45**, 1265–1277 (2020)
17. Wang, W., Tian, G., Chen, M., Tao, F., Zhang, C., Abdulraham, A.A., Li, Z., Jiang, Z.: Dual-objective program and improved artificial bee colony for the optimization of energy-conscious milling parameters subject to multiple constraints. J. Clean. Prod. **245**, 118714 (2020)
18. Ghoddosian, A., Pour, M., Eskandar, H.: Identification optimization cutting parameters based on ICA method in peripheral milling of thin wall. World Appl. Sci. J. **13**, 1886–1894 (2011)
19. Songtao, W., Minli, Z., Yihang, F., Zhe, L.: Cutting parameters optimization in machining thin-walled characteristics of aircraft engine architecture based on machining deformation. Adv. Inf. Sci. **4**, 244–252 (2012)
20. Qu, S., Zhao, J., Wang, T.: Experimental study and machining parameter optimization in milling thin-walled plates based on NSGA-II. Int. J. Adv. Manuf. Technol. **89**, 2399–2409 (2017)
21. Ringgaard, K., Mohammadi, Y., Merrild, C., Balling, O., Ahmadi, K.: Optimization of material removal rate in milling of thin-walled structures using penalty cost function. Int. J. Mach. Tools Manuf. **145**, 103430 (2019)
22. Cheng, D.J., Xu, F., Xu, S.H., Zhang, C.Y., Zhang, S.W., Kim, S.J.: Minimization of surface roughness and machining deformation in milling of Al alloy thin-walled parts. Int. J. Precis Eng. Manuf. **21**, 1597–1613 (2020)
23. Joshi, S.N., Bolar, G.: Influence of End Mill geometry on Milling Force and Surface Integrity while Machining Low Rigidity Parts. J. Inst. Eng. (India) C. **102**, 1503–1511 (2021)
24. Mia, M.: Mathematical modeling and optimization of MQL assisted end milling characteristics based on RSM and Taguchi method. Measurement. **121**, 249–260 (2018)
25. Bolar, G., Das, A., Joshi, S.N.: Measurement and analysis of cutting force and product surface quality during end-milling of thin-wall components. Measurement. **121**, 190–204 (2018)
26. Li, J., Yang, X., Ren, C., Chen, G., Wang, Y.: Multi-objective optimization of cutting parameters in Ti-6Al-4V milling process using nondominated sorting genetic algorithm-II. Int. J. Adv. Manuf. Technol. **76**, 941–953 (2015)
27. Kanagarajan, D., Karthikeyan, R., Palanikumar, K., Davim, J.P.: Optimization of electrical discharge machining characteristics of WC/Co composites using non-dominated sorting genetic algorithm (NSGA-II). Int. J. Adv. Manuf. Technol. **36**, 1124–1132 (2008)
28. Sastry, K.: Single and Multi Objective Genetic Algorithm Toolbox for MATLAB in C++ (IlliGAL Report No. 2007017), University of Illinois at Urbana-Champaign, Urbana, IL, (2007)
29. Joshi, S.N., Pande, S.S.: Intelligent process modeling and optimization of die-sinking electric discharge machining. Appl. Soft Comput. **11**, 2743–2755 (2011)
30. Vukman, J., Lukic, D., Borojevic, S., Rodic, D., Milosevic, M.: Application of fuzzy logic in the analysis of surface roughness

of thin-walled aluminum parts. Int. J. Precis Eng. Manuf. **21**, 91–102 (2020)

31. Izamshah, R., Mo, J.P.T., Ding, S.: Hybrid deflection prediction on machining thin-wall monolithic aerospace components. Proc. Inst. Mech. Eng. B J. Eng. Manuf. 226, 592–605 (2012)